Simulation of energy recovery on water utility networks by a micro-turbine with counter-rotating runners.

L Andolfatto[1], E Vagnoni[1], V Hasmatuchi[2], C Münch-Alligné[2] and F Avellan[1]

[1] École polytechnique fédérale de Lausanne, Laboratory for Hydraulic Machines, Avenue de Cour 33 bis, 1007 Lausanne, Switzerland

[2] University of Applied Sciences Valais, Route du Rawyl 47, 1950 Sion, Switzerland

E-mail: loic.andolfatto@epfl.ch

Abstract. Wherever relief valves and other energy dissipation devices are installed to limit the pressure, water utility networks provide unexploited hydropower potentials. This is mainly due to a lack of economically viable technologies for energy recovery in the pico and micro hydropower range below 100 kW. Micro-turbine with counter-rotating runners proved suitable to harvest these potentials with limited investments and almost no environmental impact. An appropriate command strategy must therefore be applied to maximize the recovered energy.

This paper deals with the construction of a Virtual Energy Recovery Station (VERS) model to simulate the energy recovery on a given installation site. It includes models of the turbine, of the water consumption and it allows to implement various command strategies. The VERS can serve various purposes. The fine tuning of the command algorithm for a specific installation site is demonstrated in the paper.

1. Introduction

In hilly or mountainous area, the difference of altitude between spring catching areas or fresh water reservoirs and water consumption areas sometimes impose to regulate the pressure in the consumption area. A relief valve is installed to keep the pressure at p_{reg} in the consumption area, as pictured in Figure 1.

Then, with a discharge Q in the pipe, the hydraulic power P_h dissipated by the valve is given by:

$$P_h = \rho\, Q \left(gH - k_{eq} \frac{Q^2}{2} - \frac{p_{reg}}{\rho} \right) \tag{1}$$

with H the gross head, k_{eq} the equivalent loss coefficient of the head water infrastructure, ρ the density of the fluid and g the gravity. Instead of dissipating this power, it can be recovered to produce electricity with an appropriate power plant, as pictured in Figure 1. The environmental impact related to the energy produced by this mean can reach negligible levels as it uses already existing infrastructures.

Many successful application of energy recovery on water utility networks have been reported [1]. But the limited revenues generated by the power station allow to reach economical

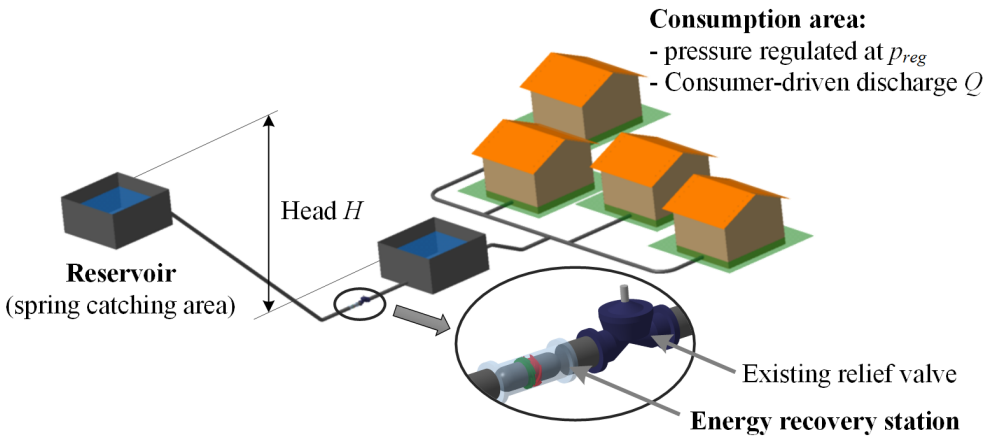

Figure 1. Water utility network with hydro power potential.

viability only when the available power is higher than a given threshold related to the capital expenditure for the installation and its operating cost.

The concept of micro-turbine with counter-rotating runners pictured in Figure 2 and presented in depth in [2, 3] is a candidate for energy recovery on drinking water network, even for an available power in the range of 5 kW to 25 kW. It features a compact axial architecture ensuring a lean in-line installation on existing facilities, therefore limiting the capital expenditure and the environmental impact of the infrastructure. Such a machine operated at variable speed can cover a wide operating domain to fit with the need of installations with uncontrolled consumer-driven flow discharge. Using a variable speed ratio between the two runners also enhances the overall efficiency of the machine [4], increasing the expected revenues.

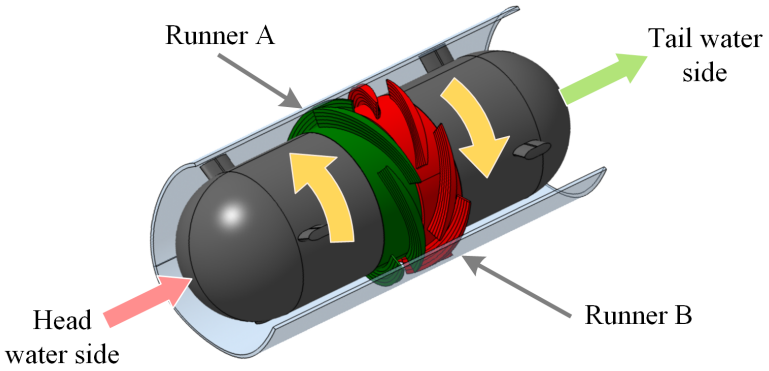

Figure 2. Axial micro-turbine with counter-rotating runners.

In order to maintain the machine cost and the maintenance cost as low as possible, the micro-turbine is commanded with a Maximum Power Point Tracking (MPPT) algorithm. It allows to avoid monitoring the operating conditions of discharge and available head and thus saving on the associated sensors. The principle of the MPPT is described in section 2.

To find the optimum values of the MPPT parameters, the entire Energy Recovery Station system is modeled and simulated. A stochastic process modeling the consumer-driven discharge of an instrumented pilot site is built. Discharge trajectories can be generated to estimate

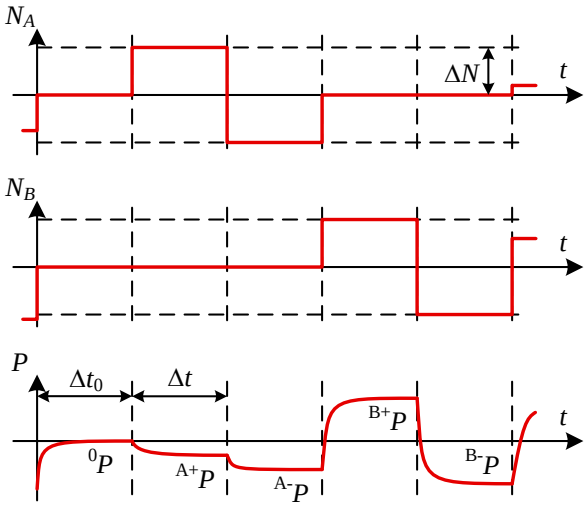

Figure 3. Chronogram of a *perturb and observe* cycle of the MPPT.

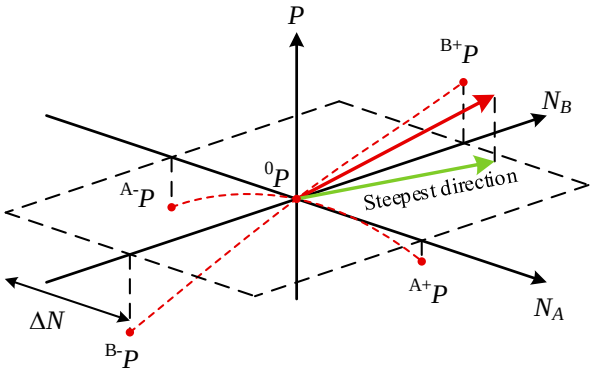

Figure 4. Estimation of the steepest direction according to the observed output power.

the energy recovered with the micro-turbine with various MPPT settings. The simulation is presented in section 3 and the results obtained are detailed in section 4.

2. Maximum Power Point Tracking command

2.1. Principle

The principle of Maximum Power Point Tracking has been initially proposed by Cherdak and Douglas [5] to control the output voltage of power sources in order to maximize the output power. It consists in applying a perturbation to the controllable parameters of the system while observing the associated alteration of the output power, what is sometimes refereed to as *perturb and observe*. The controller moves in the steepest gradient direction to improve the output power. It has been widely implemented for the control of photovoltaic system [6]. This solution has been derived for small hydro applications, such as the one proposed by Borghetti et al. [7] for instance.

As far as the micro-turbine is concerned, the controllable parameters are the two runners rotational speed, denoted N_A and N_B respectively. The output power P is the sum of the power P_A and P_B delivered by the generators coupled to the two runners. The rotational speeds are perturbed by ΔN in the positive and negative directions and the associated output power are recorded, according to the chronogram of Figure 3. The steepest direction $\boldsymbol{\nabla P}$ is determined using eq. (2).

$$\boldsymbol{\nabla P} = \begin{pmatrix} \dfrac{\partial P}{\partial N_A} \\ \dfrac{\partial P}{\partial N_B} \end{pmatrix} \tag{2}$$

Then the new set point for the time step i is computed using the direction $\boldsymbol{d}_i$ as defined in eq. (3):

$$\boldsymbol{N}_i = \begin{pmatrix} N_A \\ N_B \end{pmatrix}_i = \boldsymbol{N}_{i-1} + \alpha \cdot \boldsymbol{d}_i = \boldsymbol{N}_{i-1} + \alpha \cdot (\boldsymbol{\nabla P}_{i-1} + \beta \cdot \boldsymbol{d}_{i-1}) \tag{3}$$

Table 1. Parameters of the MPPT algorithm.

Parameter	Unit	Description
Δt	[s]	Duration of the period at current operating set point $\boldsymbol{N}_i$
Δt_0	[s]	Duration of the period at each perturbed operating set point
ΔN	[min^{-1}]	Magnitude of the rotational speed perturbation
α	[$\text{W}^{-1}\text{min}^{-2}$]	Magnitude of the set point step in the direction $\boldsymbol{d}_i$
β	[$-$]	Conjugate gradient parameter for the direction $\boldsymbol{d}_i$ computation

To keep the implementation simple and limit the resources required for an embedded controller, all the parameters summarized in Table 1 are considered to be fixed once for all. The effect of each parameter is investigated in the following sections. Apart from these parameters, the other degree of freedom in the MPPT design investigated in this paper is the method used to compute the steepest direction $\boldsymbol{\nabla P}$. First and second orders approximations are explained in subsections 2.2 and 2.3 respectively.

2.2. First order MPPT

Considering the output power as locally linear is a simple and straightforward approach to estimate its gradient. The central difference scheme of eq. (4), with the notations from Figure 3, directly provides the steepest direction.

$$\boldsymbol{\nabla P} = \frac{1}{2\Delta N} \begin{pmatrix} {}^{A+}P - {}^{A-}P \\ {}^{B+}P - {}^{B-}P \end{pmatrix} \tag{4}$$

2.3. Second order MPPT

As the gradient is likely to be estimated in neighborhood of local optima, as in Figure 4 for the runner A, the first order approach may lead to incorrect estimations. A second order approximation as defined in eq. (5) is therefore also investigated.

$$P(\boldsymbol{N} + \boldsymbol{\Delta N}) = P_0 + \boldsymbol{\Delta N}^T \cdot \begin{pmatrix} a \\ b \end{pmatrix} + \boldsymbol{\Delta N}^T \cdot \begin{pmatrix} c & e/2 \\ e/2 & d \end{pmatrix} \cdot \boldsymbol{\Delta N} \tag{5}$$

The coefficient e cannot be identified as the perturbation $\boldsymbol{\Delta N}$ only involves one runner at a time. The others coefficients are identified by solving the least square problem of eq. (6).

$$\varepsilon = \sum \left({}^{k}P - P(\boldsymbol{N} + {}^{k}\boldsymbol{\Delta N}) \right)^2 , \; k \in \{A+, A-, B+, B-\} \tag{6}$$

The gradient is finally obtained according to the expression of eq. (7).

$$\boldsymbol{\nabla P} = \begin{pmatrix} a \\ b \end{pmatrix} \tag{7}$$

This generic formulation requires more computing efforts than the first order but it is also more robust in the neighborhood of the operating domain boundaries where all the ${}^{k}\boldsymbol{\Delta N}$ are not accessible and some alternative perturbations must be used.

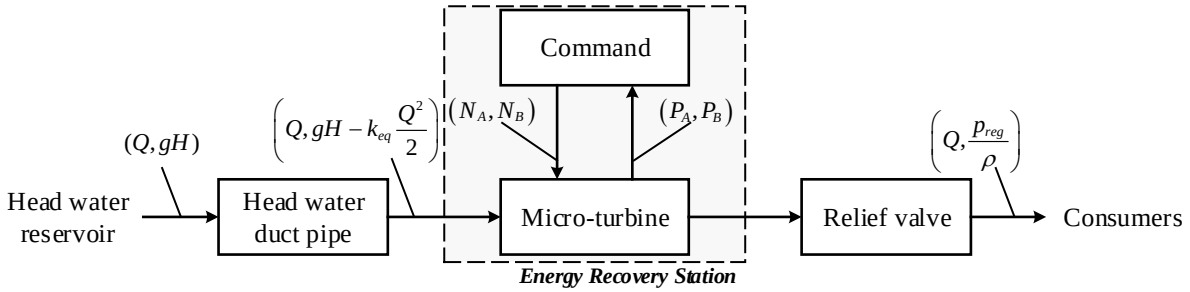

Figure 5. Energy Recovery Station within its environment.

3. Simulation of the Energy Recovery Station

3.1. Description of the system

The primary function of the water utility network consists in delivering water to consumers. This function is characterized by a target pressure p_{reg} at the tail water side of the relief valve and a discharge Q that is consumer-driven. The water is conveyed from a head water reservoir to the relief valve chamber through a duct pipe characterized by its equivalent losses coefficient k_{eq}. Then, the command for micro-turbine runners rotational speeds N_A and N_B must be computed in order to maximize the sum of the output power P_A and P_B from the two generators. To keep the pressure higher or equal to p_{reg} at the inlet of the relief valve, the maximum specific energy that can be extracted by the micro-turbine E_{av} is defined by:

$$E_{av} = gH - k_{eq}\frac{Q^2}{2} - \frac{p_{reg}}{\rho} \tag{8}$$

This is summarized in Figure 5. The net head H and the equivalent losses coefficient k_{eq} can be analytically computed according to the characteristics of the installation. Alternatively, they can be identified from on site measurements as in [4]. In order to simulate the system, the proposed analytic model of the micro-turbine and stochastic model of the consumer-driven discharge are presented in the following subsections.

3.2. Analytic model of the micro-turbine

The simulation of the system is based on a model of the micro-turbine that predicts the output power P – sum of P_A and P_B – as a function of the discharge Q and of the velocity set point $\boldsymbol{N}$. Additionally,the extracted specific energy is also estimated in order to check that the constraint on the tail water pressure is satisfied.

An experimental campaign – explained in depth in [4] – is conducted on a laboratory test rig in order to build such a model of a micro-turbine prototype. The entire operating range from N_{min} to N_{max} on both runners is explored at $n+1$ levels of extracted specific energy $\mathcal{E} = \{E_0, \ldots, E_n\}$. Analytic models based on Hermite polynomials interpolation are build accordingly:

- for the discharge passing through the micro-turbine : $\{Q_{E_i}(\boldsymbol{N})\}_{E_i \in \mathcal{E}}$.
- for the output power of the first runner : $\{P_{A,E_i}(\boldsymbol{N})\}_{E_i \in \mathcal{E}}$;
- for the output power of the second runner : $\{P_{B,E_i}(\boldsymbol{N})\}_{E_i \in \mathcal{E}}$;

The discharge models have their values sorted according to the specific energy level, as defined in eq. (9).

$$\forall \boldsymbol{N} \in [N_{min}, N_{max}]^2,\ E_i > E_j \Longleftrightarrow Q_{E_i}(\boldsymbol{N}) > Q_{E_j}(\boldsymbol{N}) \tag{9}$$

This property is exploited in the step (a) of the algorithm detailed in Figure 6. The estimated level of extracted specific energy E_{est} is estimated thanks to a linear interpolation in step (b) and (c). The output power P_A and P_B are then predicted accordingly in step (d).

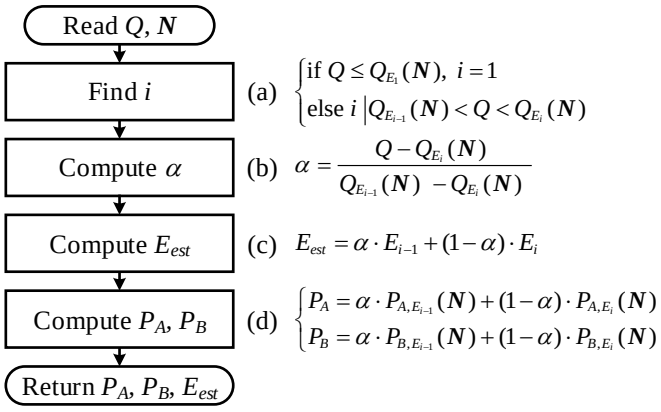

Figure 6. Prediction of the output power P_A and P_B according to the discharge Q and of the velocity set point $\boldsymbol{N}$.

A similar approach is also used to correct the ascent direction $\boldsymbol{d}_i$ of the MPPT in order to satisfy the constraint $E_{est} < E_{av}$. Nonetheless, this is not detailed in this paper.

3.3. Stochastic model of the discharge

To complete the proposed framework for the simulation of the energy recovery, the consumer-driven discharge is also modeled so that realistic time series trajectories $\{Q(k\cdot\delta t)\}_{k\in\{1,\dots,T\}}$ can be generated.

The model of time varying discharge must cope with fluctuations in the consumption at various time scale: seasonal, intra-week, intra-day and instantaneous. As the simulations aims at estimating integral quantities such as the energy production over a given period for instance, the average of the simulated discharge time series must also be unbiased.

Developing a multi-agent model considering each individual consumer or batches of consumers as proposed by Davis [8] is theoretically possible but requires a huge amount of information about the network. The global approach considering the discharge as a stochastic process is preferred, as it only requires some measured time series to be tuned. Even if auto-regressive moving-average models (ARMA) are not reported as the most efficient for monthly prediction of the discharge [9], they are selected for their versatility when it comes to short δt period of around one second as in this work.

ARMA is a popular model for stationary hydrologic time series [9]. The eq. (10) provides the formulation defined by Whittle [10].

$$Q(t_j) = \varepsilon_j + \sum_{i=1}^{p} \varphi_i \cdot Q(t_{j-i}) + \sum_{i=1}^{q} \theta_i \cdot \varepsilon_{j-i} \tag{10}$$

The model is characterized by its auto-regressive order p, its moving-average order q, its coefficients φ_i and θ_i. The random variable ε_k is a white noise. The identification of the model is made by maximizing the corrected Akaike information criterion $AICc$ [11]:

$$AICc = 2k - 2\ln L + \frac{2k(k+1}{n-k-1} \tag{11}$$

with $k = p+q+1$, n is the number of points in the measured time series and L is the likelihood of the modeled time series with respect to the measured one.

To capture the discharge fluctuation both at the daily scale and at the second scale, two sets of measurements have been performed on an instrumented pilot site. The first data set $\mathcal{Q}_{15} = \{Q_{15,k}\}_{k\in\{1,\dots,35'040\}}$ covers one year from June 2014 to June 2015 and provides the average discharge on the 35'040 periods of 15 minutes. A sample along 14 days is pictured

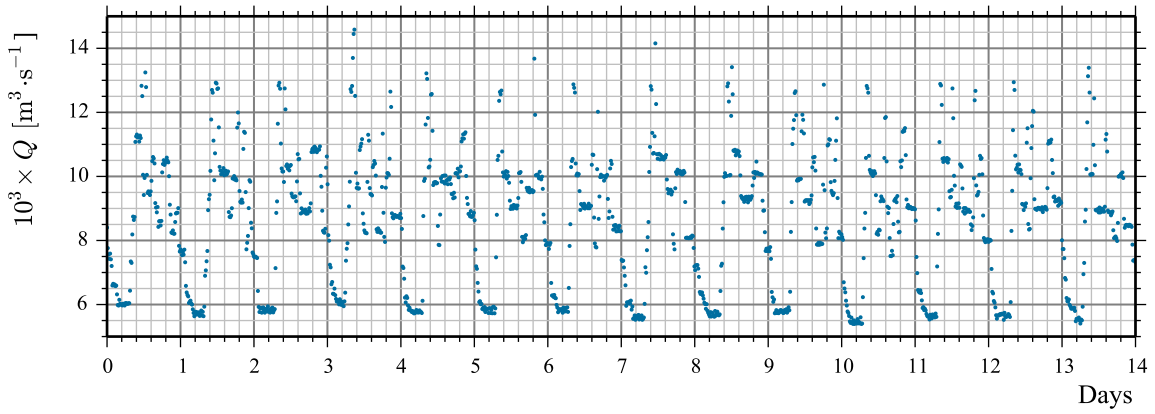

Figure 7. Sample of the 15 minutes averaged measured discharge during 14 days.

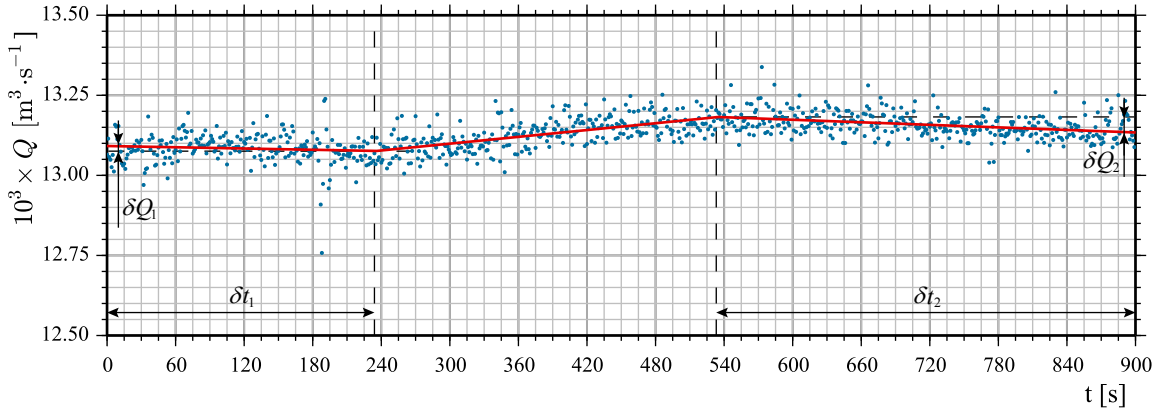

Figure 8. Sample of the instantaneous discharge measured over 15 minutes.

in Figure 7. The second data set $\mathcal{Q}_1 = \{Q_{1,m}\}_{m\in\{1,\ldots,86'400\}}$ covers one day in June 2015 and provides the instantaneous discharge with a 1 Hz acquisition frequency. A sample along 15 minutes is pictured in Figure 8. Two separate models have been build and merged to yield the stochastic model of the consumer-driven discharge.

The average value of any contiguous subset of the measured average discharge $\mathcal{Q}_{15}$ is not constant as some periodical fluctuations are experienced. It is therefore not stationary and can not be modeled directly with an ARMA model. In order to overcome this hurdle, the eq. (12) provides a multiscale model accounting for the periodical fluctuations.

$$Q_{15}(t) = \overline{Q} + Q_s(t) + Q_d(t) + Q_h(t) + w_s(t) \cdot w_d(t) \cdot w_h(t) \cdot q_{15}(t) \tag{12}$$

The discharge trend functions Q_s, Q_d, and Q_h are periodic with a mean value equal to zero over their period and they are constant over each of their sub-periods. The weight functions w_s, w_d, and w_h are periodic with a mean value equal to one over their period and they are constant over each of their sub-periods. Characteristics of these functions are detailed in the Table 2. They are iteratively identified – from the seasonal trend to the hourly trend – to match mean values and standard deviations of the measured discharge $\mathcal{Q}_{15}$. The residual q_{15} finally follows a stationary time series. It is modeled with an ARMA process.

Table 2. Characteristics of the periodical discharge trend and weight functions.

Trend	Functions	Period	Sub-period
Seasonal	Q_s, w_s	1 year	1 week
Daily	Q_d, w_d	1 week	1 day
Hourly	Q_h, w_h	1 day	1 hour

The second data set $\mathcal{Q}_1$ is used to identify the values of the time series within each period of 15 minutes previously defined. A piecewise linear trend $Q_{pl,k}(t)$ is identified on each subset of $\mathcal{Q}_1$ covering 15 minutes. The trend and its four parameters are pictured in Figure 8. The mean value of $Q_{pl,k}$ equals the mean discharge $Q_{15,k}$ obtained thanks to eq. (12) and the continuity with the previous period is ensured by imposing $Q_{pl,k}(0)$. A composed distribution $\mathcal{C}$ for the parameters $\delta t_{1,k}$, $\delta t_{2,k}$, $\delta Q_{1,k}$ and $\delta Q_{2,k}$ is identified according to $\mathcal{Q}_1$. Then, the stochastic model of the discharge is finally given by eq. (13).

$$Q(t) = Q_{pl,k}(t) + \cdot Q_f(t) \tag{13}$$

The residual instantaneous fluctuations Q_f can be considered as a stationary time series. It is therefore possible to model it with an ARMA process.

Finally, the generation of a time series for simulation purpose is sequential. First, a future trajectory generated from the ARMA model of q_{15} is transformed thanks to eq. (12) providing mean values over 15 minutes for generated time series $\mathcal{Q}_g$. Then, for each time step, a set of trend parameters $\delta t_{1,k}$, $\delta t_{2,k}$, $\delta Q_{1,k}$ and $\delta Q_{2,k}$ is drawn from the composed distribution $\mathcal{C}$ to form the trend and the final time series is obtained thanks to the generation of a future trajectory from the ARMA model of Q_f, according to eq. (13).

3.4. Implementation

All the elements described in the previous subsections have been implemented in Python [12]. The statistical analysis and the identification of the ARMA models relies on the OpenTURNS library [13]. The time step for the simulation has been set to one second. Simulation results are shown in Figure 9, where the rotational speeds are following the discharge fluctuation to track the best output power setting.

4. Results

For both first and second order gradient method, the optimum MPPT parameters have been searched considering.

- $\beta = 0$ to evaluate the relevance of a direct use of the steepest direction;
- $\beta = 0.15$ to estimate the impact of introducing the conjugate gradient.

For the four cases addressed, Δt_0, Δt, ΔN and α have been optimized in order to maximize the mean daily energy production $\overline{W}$. It has been estimated according to simulation running on one year, with the same trajectory of consumer-driven discharge.

The results are presented in Table 3.

Even though the conjugate gradient and the second order provide the best performance, the differences are almost negligible. In terms of MPPT parameters selection, the four cases also led to similar results.

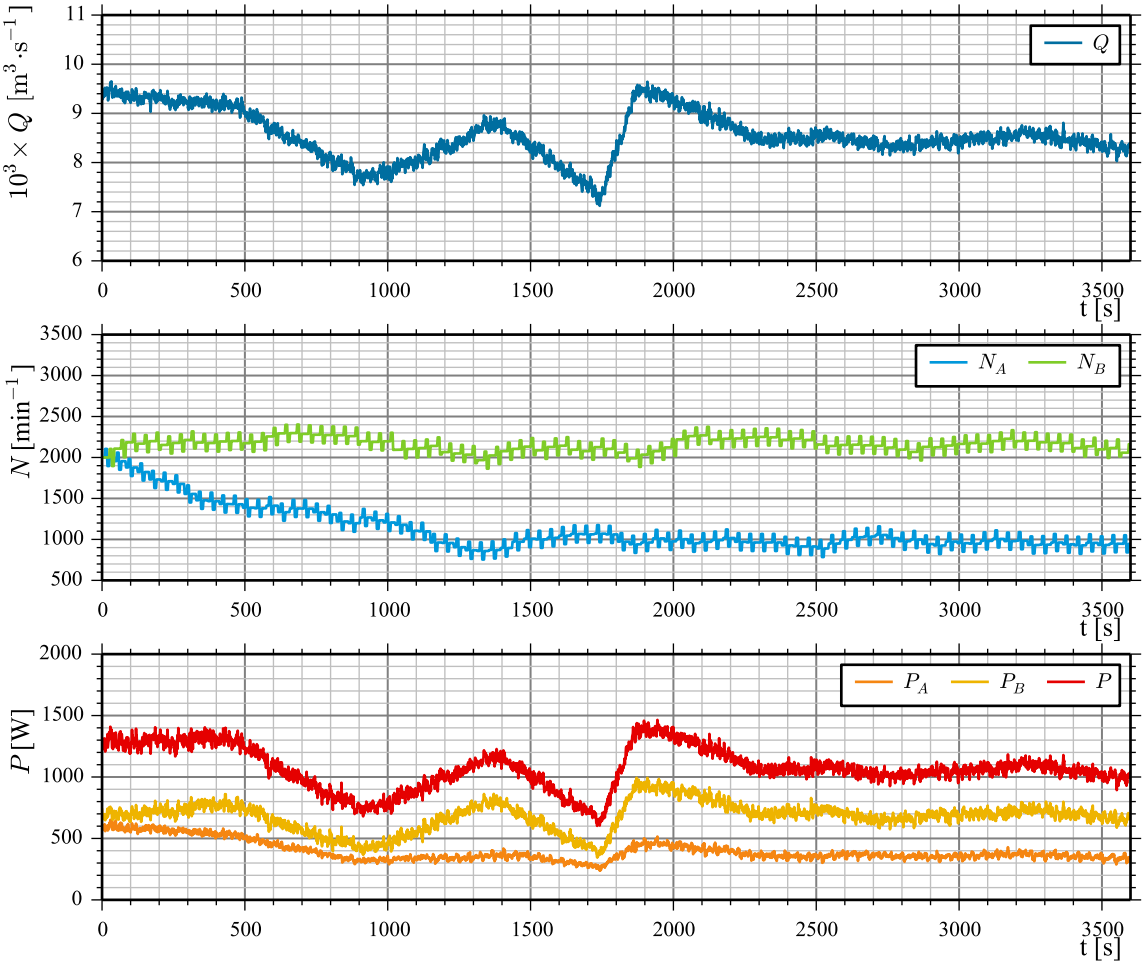

Figure 9. Simulation of the first 3600s after a start at $\boldsymbol{N} = (2000, 2000)$.

Table 3. Optimal parameters of the MPPT and associated mean daily energy production $\overline{W}$.

Order [−]	β [−]	Δt_0 [s]	Δt [s]	ΔN [min^{-1}]	α [W^{-1}min^{-2}]	$\overline{W}$ [kWh]
1	0	8.935	7.833	104.690	259.631	19.610
2	0	8.934	7.833	104.690	259.631	19.617
1	0.15	8.937	7.832	104.690	259.631	19.611
2	0.15	8.936	7.833	104.690	259.631	19.618

5. Conclusion

The design of a system dedicated to energy recovery on existing infrastructure requires to consider typical constraints that are not experienced in the case of conventional hydropower infrastructures. This paper addresses the energy recovery in drinking water networks, where the primary function of the infrastructure is to deliver water to consumers. The primary function must be preserved at all time and the Energy Recovery Station must be designed consequently.

A complete simulation framework is proposed in order to validate and to tune the command

strategy of the Energy Recovery Station. It is fueled by a discharge time series generator to reproduce the behavior of consumers with specific statistical characteristics. A MPPT command algorithm to control a micro-turbine with counter-rotating runners is presented. The performance of the system is estimated and tuned according to the characteristics of an identified pilot site.

The successful use of the proposed approach for the dedicated tuning of a station for an identified site should not hide the actual potential of the proposed approach. A similar framework can also be applied to simulate the operation of several station on a water utility network. Other components, such as intermediate reservoirs or pumps, can also be modeled on the same principal, allowing to simulate a cluster of small hydropower devices connected to a smart energy network.

Acknowledgment

The research leading to the results published in this paper has received funding from the Swiss Competence Center for Energy Research *Supply of Electricity* (SCCER SoE) granted by the Swiss Commission for Technology and Innovation (CTI); the Ark, the foundation for innovation of Valais Canton and from the Swiss Commission for Technology and Innovation as part of the DuoTurbo project number 17197.1 PFEN IW. The authors would also like to thank the implementation partners Jacquier-Luisier SA, Valelectric SA and Telsa SA for their commitment and their support in the DuoTurbo project.

References

[1] Hintermann M 1994 L'eau potable génératrice d'électricité: Inventaire et étude du potentiel des usines électriques sur l'alimentation en eau potable en suisse SFOE DIANE 10 publication URL `http://www.bfe.admin.ch/kleinwasserkraft/03834/04171/index.html?lang=en`

[2] Münch-Alligné C, Richard S, Meier B, Hasmatuchi V and Avellan F 2014 Numerical simulations of a counter-rotating micro-turbine *Advances in Hydroinformatics* Springer Hydrogeology ed Gourbesville P, Cunge J and Caignaert G (Springer Singapore) pp 363–373 ISBN 978-981-4451-41-3

[3] Andolfatto L, Euzenat C, Vagnoni E, Münch-Aligné C and Avellan F 2015 A mixed standard/custom design strategy to minimize cost and maximize efficiency for picohydro power potential harvesting *5th International Youth Conference on Energy (IYCE), 2015* pp 1–8

[4] Andolfatto L, Delgado J, Vagnoni E, Münch-Aligné C and Avellan F 2015 Analytical hill chart towards the maximisation of energy recovery on water utility networks with counter rotating micro-turbine *36th IAHR World Congress, The Hague, The Netherlands* iSBN: 978-90-824846-0-1

[5] Cherdak A S and Douglas J L 1971 Maximum power point tracker uS Patent 3,566,143 URL `https://www.google.com/patents/US3566143`

[6] Salas V, Olas E, Barrado A and Lzaro A 2006 *Solar Energy Materials and Solar Cells* **90** 1555 – 1578 ISSN 0927-0248

[7] Borghetti A, Di Silvestro M, Naldi G, Paolone M and Alberti M 2008 Maximum Efficiency Point Tracking for Adjustable-Speed Small Hydro Power Plant *16th Power Systems Computation Conference (PSCC'08)*

[8] Davis D 2000 *Computers, Environment and Urban Systems* **24** 173 – 190 ISSN 0198-9715

[9] Wang W C, Chau K W, Cheng C T and Qiu L 2009 *Journal of Hydrology* **374** 294 – 306 ISSN 0022-1694

[10] Whittle P 1951 *Hypothesis testing in time series analysis* vol 4 (Almqvist & Wiksells)

[11] Cavanaugh J E 1997 *Statistics & Probability Letters* **33** 201 – 208 ISSN 0167-7152

[12] Python Software Foundation Python language reference, version 2.7 Available at http://www.python.org

[13] OpenTURNS: an Open source initiative for the Treatment of Uncertainty, Risks'N Statistics http://doc.openturns.org/openturns-latest/sphinx/contents.html, Consulted in January 2016.